Z. Phys. C. – Particles and Fields 37, 337–345 (1988)

Zeitschrift für Physik C Particles and Fields

Neutral strange particle production in high transverse momentum π^- nucleus interactions at ~ 40 GeV/c

RISK Collaboration

H. Bärwolff, C. Dreher, W. Friebel, U. Gensch, H.E. Roloff, H.J. Schreiber, C. Spiering
Institute for High Energy Physics, DDR-1615 Berlin-Zeuthen

E. Denes, L. Diosi, T. Gemesy, L. Jenik, J. Krasznovsky, Gy. Pinter, I. Wagner
Central Research Institute for Physics, H-1088 Budapest, Hungary

A.V. Bannikov, J. Boehm, Yu.V. Grishkevich, B.A. Khomenko, Z.V. Krumstein, Yu.P. Merekov, V.I. Petrukhin, K. Safarik, G.A. Shelkov, L.G. Tkachev, L.S. Vertogradov
Joint Institute for Nuclear Research, SU-141980 Dubna, USSR

T. Soukup, A. Valkarova, S. Valkar, P. Zavada
Institute of Physics of Charles University, CS-18000 Prague, CSSR

V.G. Kristeva, V.N. Penev, A.I. Sklovskaja
Institute for Nuclear Research and Nuclear Energy, Sofia, Bulgaria

A.K. Javreishvili, A.I. Kharchilava, T.A. Lomatadze
Institute of Physics, SU-380086 Tbilisi, USSR

W. Dominik, J. Gajewski, S. Majewski, K. Pniewska, L. Ropelewski, J.A. Zakrzewski
Institute of Experimental Physics, Warsaw University, PL-00681 Warsaw, Poland

Received 4 August 1987; in revised form 25 October, 1987

Abstract. Measurements of K_s^0, Λ and $\bar{\Lambda}$ production in π^- nucleus (C, Cu, Pb) interactions are presented. The experiment was carried out with the streamer chamber spectrometer RISK using a π^- beam of ~ 40 GeV/c and a trigger requiring a secondary charged particle with transverse momentum above 1.1 GeV/c. Production cross sections, relative production rates and distributions of Feynman x and transverse momentum squared as well as correlations between the V^0 and the trigger particle are presented. The results are compared and found to be in agreement with K_s^0, Λ and $\bar{\Lambda}$ data from untriggered $\pi^- p$ and $\pi^- C$ interactions, except for the relative production rate of antilambdas which is about to times larger in high-p_t collisions. Our results can be well interpreted within the dual topological unitarization model.

1 Introduction

In this paper neutral strange particle production in high transverse momentum π^--nucleus collisions at a beam momentum of ~ 40 GeV/c is investigated. In studies of hadron-hadron scattering only asymptotic states are measured and very little insight into the nature of hadronic matter at the time of its creation exists. It is however possible to affect the early stages of an interaction and learn about hadronic matter at nascendy by using nuclear targets. When a high-energy projectile collides with a nucleus and interacts with one of the nucleons, the remaining nucleons serve as secondary targets for reinteractions of the states produced in the initial collisions. By varying the atomic number of the target, differences may be observed which can be attributed to the details of

the strong interactions over short space-time intervals.

In this work we analyze V^0-events from π^--nucleus interactions selected under special triggering conditions: one of the charged secondaries produced in the central region of the πN c.m. system ($x_F = 2p_L^*/\sqrt{s} \sim 0$) has a transverse momentum above $p_t = 1.1$ GeV/c. The study of collisions producing an $s\bar{s}$-quark pair at nascendy together with a final state particle of large transverse momentum provides some challenge for current models of particle production in high energy hadron-nucleus interactions. Neutral strange particles are particularly interesting for this purpose, since their decays to charged pairs provide an excellent experimental signature for the production of strangeness over a large range of phase space.

Comparing our results with K^0's, lambdas and antilambdas produced in π^--proton [1] and π^--carbon [2] collisions in a bubble chamber at the same incident momentum may help to disentangle the underlaying production mechanisms. The hydrogen data are not affected by reinteractions while the carbon data involve possible nuclear effects. Both bubble chamber data do not involve large transverse momentum particle selection, but include effects due to the creation of an additional strange-antistrange quantum number pair.

The paper is organized as follows. Section 2 describes our apparatus and the trigger condition. The event analysis is described in Sect. 3. Section 4 presents the results for the cross sections, relative production rates, differential cross sections and correlation studies. Discussion and comparison with $\pi^- p$ and $\pi^- C$ bubble chamber data as well as with the predictions of a dual topological unitarization model are also involved in this section. Conclusions are drawn in Sect. 5.

2 Experimental set-up and trigger

The study has been performed with a streamer chamber spectrometer. The main part of the apparatus was the three gap streamer chamber RISK filled with a 50% – 50% helium-neon gas mixture at atmospheric pressure. A memory time of 1–2 μs was achieved through a small admixture of SF_6. The size of the streamer chamber ($4.7 \times 0.9 \times 0.8$ m^3) was chosen such that it fits into the magnet gap. The electrodes were constructed by stainless wire meshes with a transparency of 85%. A Marx-generator provided via a bipolar Blumlein-line the high voltage pulse of about ± 400 kV height and 19 ns duration.

The sensitive volume of the chamber was viewed by eight lenses each equipped with two-stage image intensifiers. Details on the chamber, the high voltage system and the optics may be found elsewhere [3–5].

The streamer chamber was positioned in a ~ 1.5 T magnetic field. The main field component normal to the film plane was known with an accuracy better than 0.5%. The other two components were negligible within the visible chamber volume.

The chamber was exposed at the Serpukhov proton synchrotron to an unseparated beam of negatively charged particles with a mean momentum of 38 GeV/c and with an intensity of $\sim 3 \cdot 10^5$ particles in a 0.5 s spill. The beam spot at the entrance window of the chamber was defined by a telescope of scintillation counters. The identification of the beam particles was achieved by a set of four threshold Cherenkov

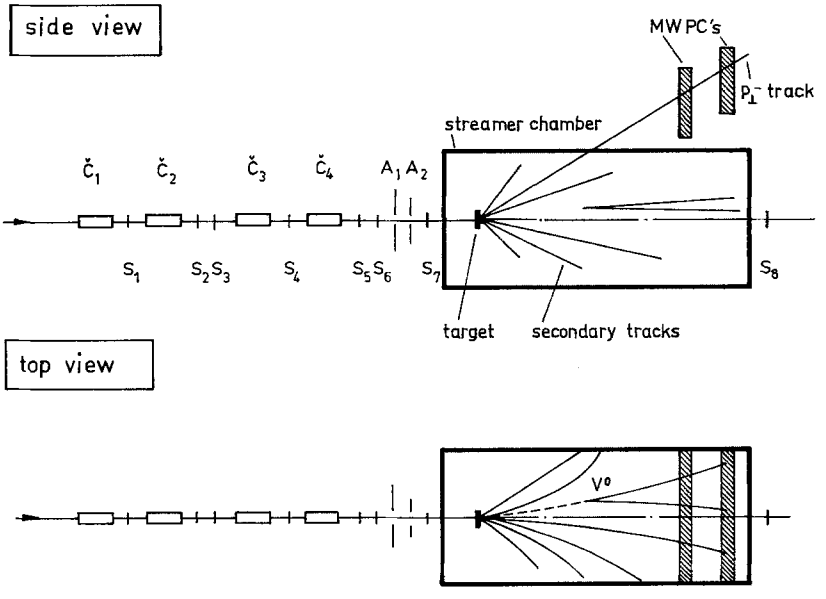

Fig. 1. Schematic lay-out of the streamer chamber spectrometer RISK for the high-p_t experiment

counters. The beam composition turned out to be $\pi^-:K^-:\bar{p}=100:1.8:0.3$.

Carbon, copper and lead disks were used as targets, with pion absorption length of 1.9%, 1.3% and 0.74%, respectively. The exchangeable targets were placed in the streamer chamber about 30 cm downstream of the entrance window. To avoid discharges of the electric field of the streamer chamber the targets were contained in a small mylar box flushed by the electronegative gas freon-12.

The p_t-trigger was formed by two proportional chambers (MWPC's) placed, as seen in Fig. 1, above the streamer chamber inside the magnet 3.6 m downstream from the target. Each chamber had two sensitive planes of 3 mm pitches spaced by 16 mm measuring y- and z-coordinates. Dimensions of sensitive areas of the chambers were 1.0×0.5 m^2 (horizontal and vertical, respectively) and the distance between the chamber was 0.6 m. The MWPC-telescope covered the polar angle interval $12° < \theta < 22°$ for particles originating from the target which corresponds to $85° < \theta^* < 120°$ in the πN c.m.s. The y-hits of a particle in the MWPC's, y_1 and y_2, together with the target position allow to estimate the momentum projection in the x, y-plane, p_{xy}. If this quantity is combined with the range of the dip angle viewed by the telescope, a determination of a threshold for the transverse momentum is possible.

The total event trigger consists of the logical AND of (1) an incident beam particle; (2) an interaction in the streamer chamber by the absence of the beam particle in the downstream scintillation counter; (3) y_1 and y_2 in a region preselected by a hardwired coincidence matrix and (4) z_1 and z_2 correlated in a way to suppress background hits.

Data were taken with p_t-thresholds between 1.1 and 1.7 GeV/c.

3 Data analysis

Some 45000 photographs, nearly equally distributed on the C, Cu and Pb targets, were scanned for p_t-interactions with at least one V^0. We found 1720 event candidates. Only the high-p_t track, the V^0, the primary track and two further secondary tracks (to ensure good primary vertex reconstruction) were measured on semiautomatic devices. The events were processed through the geometrical reconstruction program HYGEOM [6] and only retained for further analysis if

(1) the momentum error of the secondaries and of the V^0-decay tracks is less than 10% and the residual (in space) does not exceed 1800 μm;

(2) the primary vertex is reconstructed within the target;

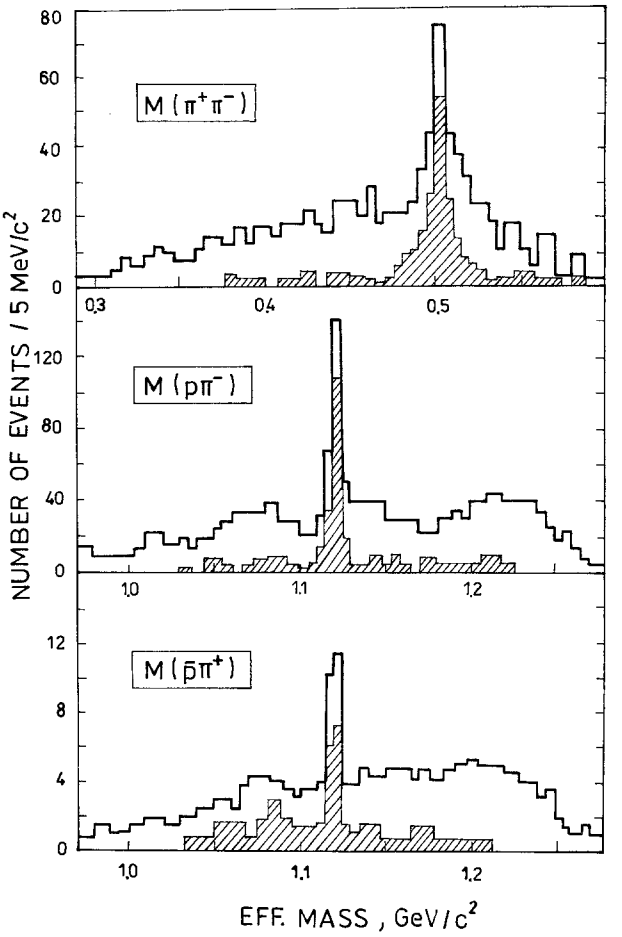

Fig. 2. Effective mass distributions $M(\pi^+\pi^-)$, $M(p\pi^-)$ and $M(\bar{p}\pi^+)$ of all V^0 candidates. The hatched histograms represent the V^0 samples after photon rejection

(3) the V^0's decay inside the fiducial volume. The cut imposes a target dependent minimum V^0-path length and a maximum downstream length of 1 m. The radius of the fiducal volume (being a zylinder) was chosen to ensure a minimum track length of 15 cm.

If an event failed the quality requirements (1) it was remeasured and reconstructed. After three unsuccessful trials it was rejected from the event sample.

To resolve the V^0/γ-ambiguity, photon conversions were rejected by demanding $M(e^+e^-) > 30$ MeV/c^2. This cut is sufficient to reject all γ's and removes less than 5% of the V^0's. Figure 2 shows the effective mass distributions $M(\pi^+\pi^-)$, $M(p\pi^-)$ and $M(\bar{p}\pi^+)$ before and after (hatched histograms) photon rejection. Clear signals for K_s^0, Λ and $\bar{\Lambda}$ particles can be seen. The widths are consistent with the detector resolution [7], while the central mass values are slightly above* the Particle Data Group values [8].

* The K_s^0 mass lies ~ 3 MeV/c^2 and the lambda mass ~ 1.5 MeV/c^2 above their respective table values. A calibration error of the magnetic field of 0.3% may account for such mass shifts [7]

Table 1. Number of K_s^0, Λ and $\bar{\Lambda}$ events observed in high-p_t $\pi^- A$ collisions at 40 GeV/c

	K_s^0	Λ	$\bar{\Lambda}$
C	75	68	12
Cu	48	96	11
Pb	41	51	8

The Λ ($\bar{\Lambda}$) sample is defined if $M(p\pi^-)$ ($M(\bar{p}\pi^+)$) is between 1.109 and 1.125 GeV/c^2. For the K_s^0 sample we required $M(\pi^+\pi^-)$ between 0.475 and 0.530 GeV/c^2 and the transverse momentum of the positive track with respect to the V^0-flight path must exceed 0.120 GeV/c. The last condition removes $\Lambda/\bar{\Lambda}$ reflections in the K_s^0 event sample. After the cuts background is negligible for the K_s^0 and lambdas, while about 15% is present in the $\bar{\Lambda}$ sample (see also Fig. 2). The V^0 mean lifetimes were measured to be $\tau_{K_s^0}=(0.91\pm0.12)\cdot10^{-10}$ s, $\tau_\Lambda=(2.67\pm0.13)\cdot10^{-10}$ s and $\tau_{\bar{\Lambda}}=(2.54\pm0.28)\cdot10^{-10}$ s, in good agreement with the Particle Data Group values [8].

The K_s^0, Λ and $\bar{\Lambda}$ event samples were checked for possible losses due to our selection criteria by analyzing the $\cos\theta_{cm}$-distribution. The angle θ_{cm} is defined as the angle between the direction of the positive decay track in the rest frame of the V^0 and the direction of the V^0 in the laboratory frame. For the Λ and $\bar{\Lambda}$, the distribution is isotropic. Some losses of K_s^0 occur near $|\cos\theta_{cm}|=1$ due to the transverse momentum cut for the positive decay track.

We conclude, the K_s^0 and Λ samples are essentially pure. Contaminations do not exceed few percent. Background of $\sim15\%$ in the $\bar{\Lambda}$ sample will be subtracted in the following analysis. Losses of K_s^0 are accounted for by requiring isotropy in the $\cos\theta_{cm}$-distribution.

Table 1 summarizes the accepted numbers of K_s^0, Λ and $\bar{\Lambda}$ (after background subtraction) for the three targets.

4 Experimental results

4.1 K_s^0, Λ and $\bar{\Lambda}$ cross sections

The cross section for the reactions

$$\pi^- + A \to K_s^0 + \text{trigger particle} + X \quad (1)$$

$$\pi^- + A \to \Lambda + \text{trigger particle} + X \quad (2)$$

$$\pi^- + A \to \bar{\Lambda} + \text{trigger particle} + X \quad (3)$$

with $A=C$, Cu or Pb and $X=$anything, are determined from the relation

$$\sigma = N/(L\cdot \text{Acc}). \quad (4)$$

Table 2. Correction factors applied in order to obtain the total number of events for reactions (1)–(3), for the three targets

		C	Cu	Pb
Scanning		1.03	1.05	1.08
Measuring and reconstruction		1.13	1.20	1.23
Fiducial volume	K_s^0	2.94	5.89	8.10
	$\Lambda/\bar{\Lambda}$	3.97	7.79	13.10
Selection criteria	K_s^0	1.95	1.95	1.96
	Λ	1.32	1.32	1.32
	$\bar{\Lambda}$	1.12	1.12	1.12
Neutral decay modes	K_s^0	1.46	1.46	1.46
	$\Lambda/\bar{\Lambda}$	1.56	1.56	1.56
Background	K_s^0	0.98	0.98	0.98
	Λ	0.97	0.97	0.97
	$\bar{\Lambda}$	0.86	0.84	0.80

N is the number of events, L the luminosity and Acc the spectrometer acceptance for the trigger particle. The number of events for reactions (1)–(3) is obtained from the selected K_s^0, Λ and $\bar{\Lambda}$ samples after background substraction and after corrections for scanning, measuring and reconstruction losses, losses due to our selection criteria, fiducial volume cuts and neutral decay modes. Table 2 lists the correction factors applied.

The spectrometer acceptance for the trigger particle, Acc, has been determined from $\pi^- A$ high-p_t V^0-events modelled by the dual topological unitarization (DTU) scheme [9]. These events were used as input for an experimental set-up simulation program. The program tracked the charged particles through the apparatus, took into account decays of neutral and charged secondaries, photon conversions and inefficiencies of the MPWC's. The hits recorded in the MWPC's were subjected to the trigger condition. The limited azimuthal angle region of the trigger particle determines mainly the spectrometer acceptance and amounts to $\sim6\%$ in the p_t-range from threshold to ~2.5 GeV/c. Other effects are less stringent, so that typical acceptance values were found to be 3–4%. The systematic uncertainty of the acceptance calculation has been estimated to be 15%*.

The luminosity L was obtained from beam monitor informations, the dead time of the apparatus and the target properties.

All cross sections were normalized to a common

* In a different estimation each DST-event has been randomly rotated around the beam direction. The ratio of the number of the events triggered to that of the rotated events determines the spectrometer acceptance for each event. Their average values agree within 10% with the results as described above. In addition, for the carbon target, bubble chamber data [2] were also used as input for the set-up simulation program. The acceptances obtained agree well with the other ones

Table 3. Cross sections for reactions (1)–(3) with a transverse momentum threshold of 1.1 GeV/c for the p_t-particle

	Cross section, mb		
	C	Cu	Pb
$\pi^- A \to K_s^0 + p_t\text{-particle} + X$	0.99 ± 0.36	4.43 ± 1.59	12.96 ± 3.92
$\pi^- A \to \Lambda + p_t\text{-particle} + X$	0.32 ± 0.12	1.73 ± 0.58	4.92 ± 1.72
$\pi^- A \to \bar{\Lambda} + p_t\text{-particle} + X$	0.03 ± 0.01	0.09 ± 0.05	0.59 ± 0.32

Table 4. Relative production rates for K_s^0, Λ and $\bar{\Lambda}$'s in $\pi^- A$ high-p_t collisions compared with those from $\pi^- p$ and $\pi^- C$ bubble chamber data

	This experiment			Bubble chamber experiment		
	$\langle n_{K_s^0} \rangle$	$\langle n_\Lambda \rangle$	$\langle n_{\bar{\Lambda}} \rangle$	$\langle n_{K_s^0} \rangle$	$\langle n_\Lambda \rangle$	$\langle n_{\bar{\Lambda}} \rangle$
Hydrogen	–	–	–	0.113 ± 0.007	0.065 ± 0.006	0.008 ± 0.002
C	0.12 ± 0.02	0.11 ± 0.02	0.019 ± 0.003	0.12 ± 0.01	0.08 ± 0.01	0.008 ± 0.001
Cu	0.18 ± 0.03	0.34 ± 0.03	0.030 ± 0.003	–	–	–
Pb	0.28 ± 0.03	0.37 ± 0.03	0.044 ± 0.004	–	–	–

trigger p_t-threshold of 1.1 GeV/c. The normalization procedure relies on inclusive transverse momentum spectra of charged particles produced under the same conditions. The spectra were simple parametrized as exponentials above the run-dependent p_t-threshold and extrapolated to $p_t = 1.1$ GeV/c. Uncertainties caused by this procedure were taken into account by an additional cross section error of 10%.

Table 3 summarizes the cross sections for reactions (1)–(3) at C, Cu and Pb targets. The minimum transverse momentum for the trigger particle is 1.1 GeV/c.

In Table 4 are presented the relative production rates for K_s^0, Λ and $\bar{\Lambda}$'s as obtained in this experiment as well as those from $\pi^- p$ and $\pi^- C$ bubble chamber experiments [2]. Apart from the general growing of $\langle n_{K_s^0} \rangle$, $\langle n_\Lambda \rangle$ and $\langle n_{\bar{\Lambda}} \rangle$ with increasing atomic weight, differences for the K_s^0 and Λ production probabilities in carbon between the triggered and untriggered interactions cannot be observed. However, $\bar{\Lambda}$'s are produced by about a factor 2 more abundantly in $\pi^- C$ high-p_t collisions. Whether this observation holds for heavier targets and also for K_s^0 and Λ's cannot be answered since minimum bias V^0 production rates are not yet available from this collaboration.

4.2 Atomic weight dependence of K_s^0, Λ and $\bar{\Lambda}$ production

The cross sections for reaction (1)–(3) as function of the atomic weight A are shown in Fig. 3. The rates for K_s^0, Λ and $\bar{\Lambda}$ production increase with increasing A and may be parametrized as

$$\sigma = \sigma_0 \cdot A^\alpha. \tag{5}$$

The fitted values for α and σ_0 are listed in Table 5. In a kinematic region in which multiple interactions are reduced (as, for example, in hadron production at large transverse momentum) perturbative QCD predicts $\sigma \propto A$, since in the impuls approximation the cross section depends on the number of quarks [10]. In practice, effects due to the nuclear environment such as Fermi motion, rescattering, and final-state interactions which occur as the quarks hadronize reduce α by 10–20% [11].

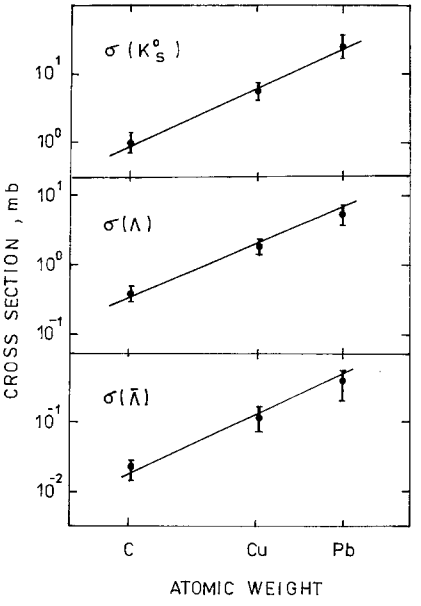

Fig. 3. Cross sections for reactions (1)–(3) at 40 GeV/c as functions of the atomic weight A

4.3. Differential K_s^0, Λ and $\bar{\Lambda}$ distributions

Figure 4 shows the Feynman x (defined in the $\pi^- N$ c.m.s.) distributions of K_s^0 producted at C, Cu and Pb targets. The K_s^0 are essentially produced in

Table 5. Values of α and σ_0 obtained from fits with the parametrization $\sigma = \sigma_0 A^{\alpha}$

	α	σ_0, mb
K_s^0	0.90 ± 0.17	0.10 ± 0.07
Λ	0.95 ± 0.16	0.03 ± 0.02
$\bar{\Lambda}$	1.02 ± 0.38	0.01 ± 0.01

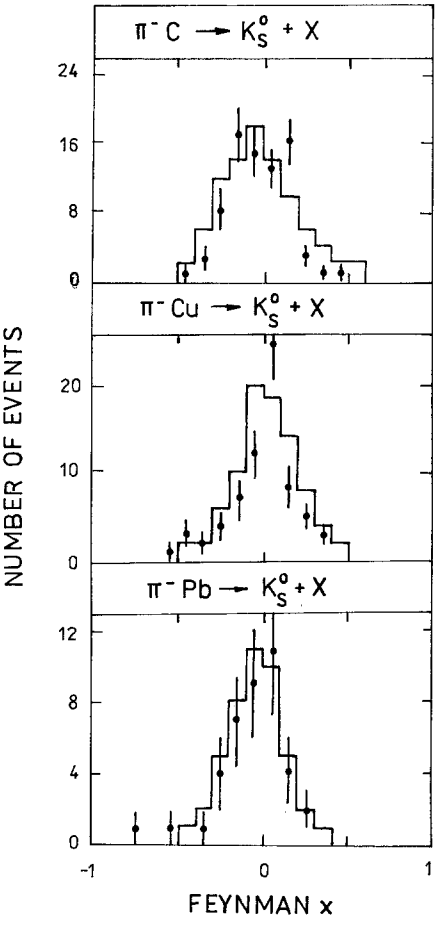

Fig. 4. Feynman x distributions of K_s^0 produced in high-p_t $\pi^- A$ collisions. The continuous histograms are the DTU predictions normalized to the data

the central region. Beam fragmentation into K^0, supported by their valence quark content, seems not be present*. An estimate of 10–20% backward produced K_s^0 is obtained when reflecting the x_F-spectra at $x_F = 0$. Such K_s^0 might be due to nucleon fragmentation into a hyperon and a kaon (with additional pions) or due to rescattering effects within the nuclei. Since backward K_s^0 production is evidently present in hydrogen interactions [1], rescattering within the nuclei

* The d-quark of the incoming π^- may be carried on the K^0 so that it might be forward produced

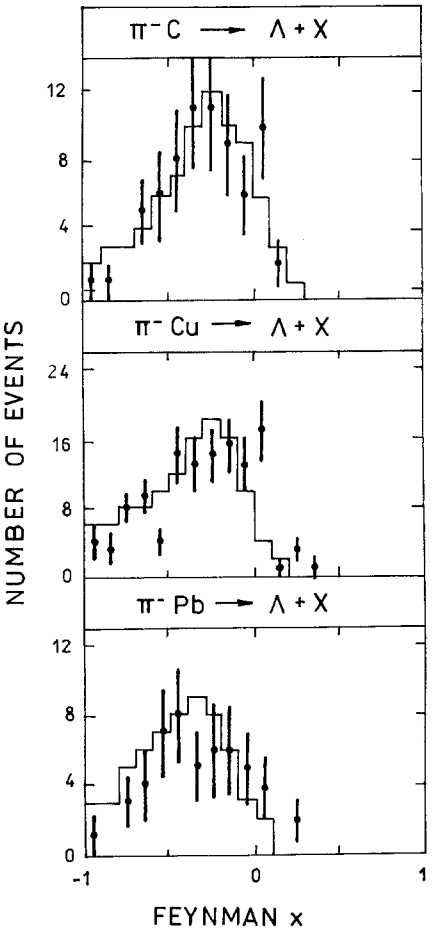

Fig. 5. Feynman x distributions of lambdas produced in high-p_t $\pi^- A$ collisions at 40 GeV/c. The continuous histograms are the DTU predictions normalized to the data

should not be solely responsible for backward produced K_s^0.

Distinct variations of K_s^0 production properties with the atomic number A cannot be observed.

Figure 5 shows the x_F-spectra of the lambdas. They are characterized by a broad bump between $-1 < x_F < 0$ with the maximum near $x_F = -0.3$, independent of the atomic number A. The lambdas are consistent with being produced as target fragmentation products. This can be well understood since the lambdas may have two quarks in common with the target nucleon.

It is interesting to note that our K_s^0 and Λ distributions are very similar to those from bubble chamber $\pi^- p$ and $\pi^- C$ data [1, 2]. The latter ones are from untriggered events while our K_s^0 and lambdas are only produced in association with a charged particle of large transverse momentum.

Figures 6 and 7 show the p_t^2-distribution for the K_s^0 and lambads, respectively. All follow an exponential form. No significant variation with the atomic

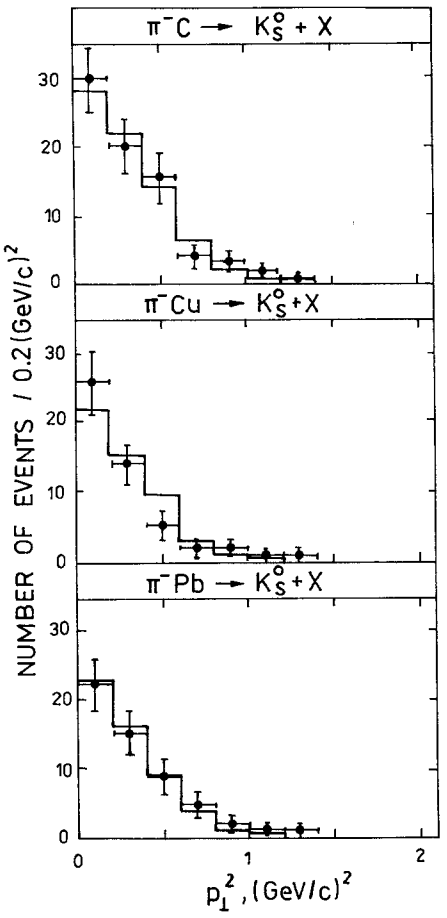

Fig. 6. Transverse momentum squred distributions for K_s^0's produced in high-p_t $\pi^- A$ interactions at 40 GeV/c. The continuous histograms are the DTU predictions normalized to the data

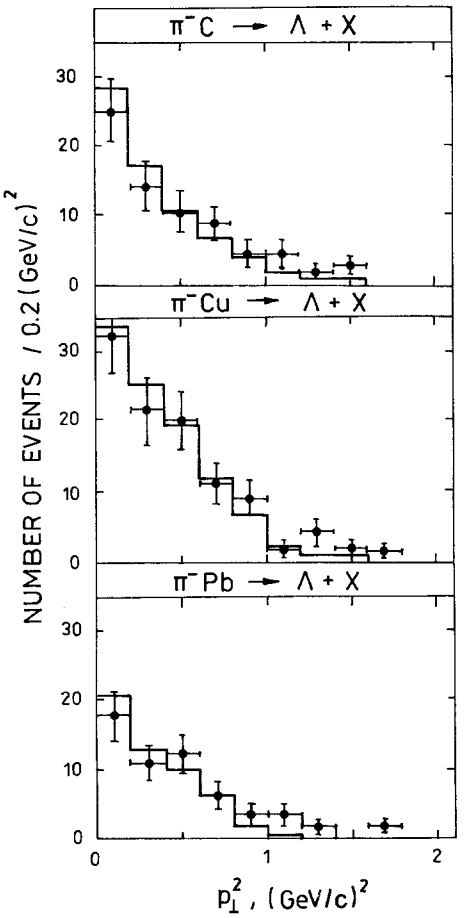

Fig. 7. Transverse momentum squared distributions for lambdas produced in high-p_t $\pi^- A$ interactions at 40 GeV/c. The continuous histograms are the DTU predictions normalized to the data

number A can be observed. It is however evident that the Λ's are produced less peripheral than the kaons.

Table 6 summarizes the average x_F-values as well as the slopes of the p_t^2-spectra obtained from exponential fits.

Figure 8 presents the x_F and p_t^2-distributions for the $\bar{\Lambda}$'s, combined for the three targets because of low statistics and negligible A-dependence for K_s^0 and Λ production. The $\bar{\Lambda}$'s are produced in the central region with a slight tendency of negative x_F. The p_t^2-spectrum falls off with an exponential slope 1.62 ± 0.41 $(\mathrm{GeV/c})^{-2}$ which seems somewhat smaller than that of the lambdas (see Table 6). A possible $\bar{\Lambda}$ production mechanism might be the formation of a central cluster which decays into a $\bar{\Lambda}\Lambda$ pair [12]. If in 80% of the cases $\bar{\Lambda}$ production proceeds via an $\bar{\Lambda}\Lambda$ pair, the expected number of such events taking into account the Λ detection probability is ~ 1, which is consistent with no $\bar{\Lambda}\Lambda$ event observed in our experiment.

It is again worthwile to note the close similarity of our $\bar{\Lambda}$ spectra with those from the 40 GeV/c bubble chamber experiments [1, 2].

Table 6. Collection of average x_F-values and slopes of exponential fits to the transverse momentum squared distributions for K_s^0, lambdas and antilambdas produced in high-p_t $\pi^- A$ interactions at 40 GeV/c

	C	Cu	Pb
$\langle x_F \rangle_{K_s^0}$	-0.01 ± 0.01	0.00 ± 0.02	-0.06 ± 0.03
$\langle x_F \rangle_{\Lambda}$	-0.25 ± 0.02	-0.30 ± 0.03	-0.32 ± 0.03
slope$_{K_s^0}$, $(\mathrm{GeV/c})^{-2}$	2.84 ± 0.37	3.40 ± 0.67	2.86 ± 0.44
slope$_{\Lambda}$, $(\mathrm{GeV/c})^{-2}$	2.10 ± 0.31	2.18 ± 0.27	2.15 ± 0.35
$\langle x_F \rangle_{\bar{\Lambda}}$		-0.18 ± 0.05	
slope$_{\bar{\Lambda}}$, $(\mathrm{GeV/c})^{-2}$		1.62 ± 0.41	

The agreement of the main properties of K_s^0 and Λ's produced in $\pi^- A$ high-p_t collisions and in untriggered $\pi^- p$ and $\pi^- C$ (soft-p_t) interactions suggests that mechanisms for the creation of a strange-antistrange particle pair, which is a common feature of the reac-

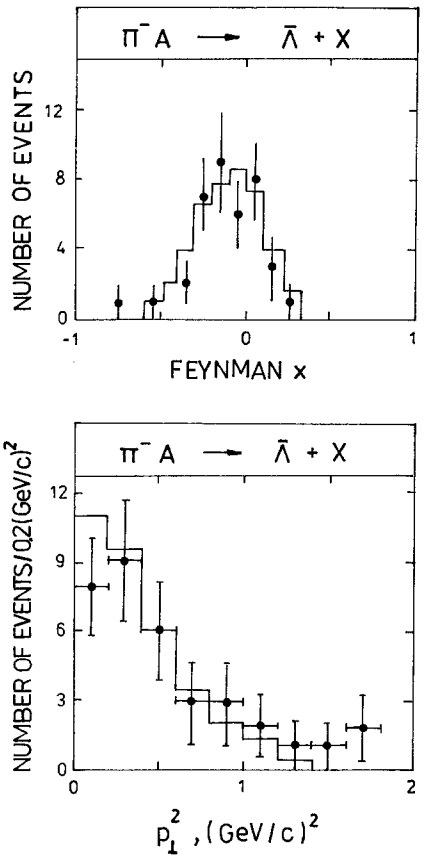

Fig. 8. Feynman x and transverse momentum squared distributions for antilambdas produced in high-p_t $\pi^- A$ interactions at 40 GeV/c. The continuous histograms are the DTU predictions normalized to the data

tions discussed, play an import role. The dual topological unitarization model (DTU) has been successfully used to describe inclusive high-energy hadron-nucleus interactions [9]. This model generates strange particles in $\pi^- A$ collisions via the creation of an $s\bar{s}$-quantum number pair (or pairs) in the quark colour field with subsequent fragmentation of the quarks into hadrons. It does not involve hard scattering processes of the hadron constituents. The DTU-spectra for K_s^0 and lambda's produced in association with a charged particle with transverse momentum above 1.1 GeV/c are shown in Figs. 4–7 as continuous histograms. Good agreement between the data and the model can be observed.

In the DTU scheme, $\bar{\Lambda}$ production is achieved in 80% of the cases via the creation of an $s\bar{s}$-quark pair and a diquark (ud)-antidiquark $(\bar{u}\bar{d})$ system which form via recombination a $\Lambda(uds)$ and an $\bar{\Lambda}(\bar{u}\bar{d}\bar{s})$. As seen in Fig. 8, such mechanism (continuous histogram) describes our $\bar{\Lambda}$ spectra reasonably well.

4.4 Correlations between $K_s^0/\Lambda/\bar{\Lambda}$ and the high-p_t trigger particle

Effective mass distributions between the V^0 and the trigger particle* were looked for resonance production. Neither significant K^* nor Σ^* resonances were observed.

Since the V^0 is often produced near $x_F = 0$ close to the trigger particle, local transverse momentum compensation between these particles may occur. Figure 9 shows the angle between the V^0 and the high-p_t track, $\phi_\perp$, in the plane perpendicular to the beam. The kaons tend to be produced back-to-back with the trigger particle, while for the lambdas and antilambdas an isotropic distribution is observed. The *DTU*-model (continuous histogram) accounts well for this different behaviour, because local transverse momentum conservation of the quark-antiquark $(s\bar{s})$ pair created manifests itself in oppositve p_t of the final hadrons, which may be sometimes the trigger particle and the kaon. For the lambdas and antilambdas,

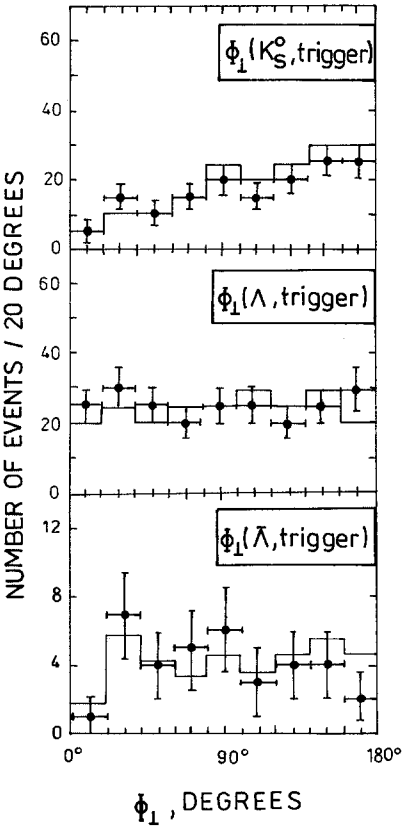

Fig. 9. Angle $\phi_\perp$, between the K_s^0, Λ *or* $\bar{\Lambda}$ and the high-p_t trigger particle in the plane perpendicular to the beam direction. The continuous histograms are the DTU predictions normalized to the data

* The pion mass has been assigned to the trigger track

which are mainly target fragmentation products respectively created mainly as $\bar{\Lambda}\Lambda$ pairs, such correlation is not expected. Similar results were found in [13] by the EHS-RCBC collaboration. This collaboration demonstrated that dynamical p_t-correlations exist for particles which originate close in rapidity space and having quantum numbers to accommodate a created $s\bar{s}$-quark pair.

5 Conclusions

We have studied the production characteristics of kaons, lambdas and antilambdas in $\pi^- A$ ($A=C$, Cu or Pb) interactions at ~ 40 GeV/c. The events were selected by triggering on a charged secondary with transverse momentum above 1.1 GeV/c at $x_F \sim 0$ in the πN c.m. system.

The K_s^0, Λ and $\bar{\Lambda}$ cross sections vary as A^α, where $\alpha \simeq 0.9$ with an error of about 20%. The relative production rates for K_s^0, Λ and $\bar{\Lambda}$'s are presented. It is found that for $\bar{\Lambda}$'s the creation probability is ~ 2 times larger in high-p_t $\pi^- C$ collisions than in untriggered inteactions.

K_s^0 and $\bar{\Lambda}$ particles are mainly produced centrally in the πN c.m.s. The Λ's are dominantly due to target fragmentation and concentrate near $x_F = -0.3$. The p_t^2-spectra of the K_s^0, Λ and $\bar{\Lambda}$ have an exponential shape and indicate in this order a less steep behaviour. For the K_s^0 and Λ's no significant shape variations with respect to the atomic number of the target are observed.

Back-to-back correlations are observed between the K_s^0 and the high-p_t trigger particle in the plane perpendicular to the beam, but not for the Λ or $\bar{\Lambda}$ particle.

The general agreement of our K_s^0, Λ and $\bar{\Lambda}$ spectra with those from untriggered (soft-p_t) $\pi^- p$ and $\pi^- C$ bubble chamber data leads us to conclude that no hard scattering effects dominate. The properties observed are consistent with being due to soft hadron production on the large transverse momentum tail.

The DTU-model which creates (di)quark-anti(di)-quark pair(s) within the colour field of the interacting partons is able to describe the properties observed. Since this model does not involve hard scattering subprocesses, additional support is obtained for our general conclusion of soft K_s^0, Λ and $\bar{\Lambda}$ production in high-transverse momentum ($p_t > 1.1$ GeV/c for at least one charged particle) π^--nuclei interactions at 40 GeV/c.

References

1. A.U. Abdurakhimov et al.: JINR, 1-6967, Dubna (1973); JINR, R1-7267, Dubna (1973); Jad. Fiz. 18 (1973) 1251; N. Angelov et al.: JINR, P1-81-5, Dubna (1981)
2. N. Angelov et al.: Jad. Fiz. 25 (1977) 350; Yad. Fiz. 24 (1976) 732; S.V. Dzhmukhadze et al.: JINR, P1-12617, Dubna (1979)
3. A.K. Javrishvili et al.: Nucl. Instrum. Methods 177 (1980) 381; G. Bohm et al.: Jad. Fiz. 35 (1982) 700
4. A.W. Bannikov et al.: Prib. Tekh. Eksp. 2 (1985) 35
5. J. Baehr et al.: preprint IHEP-Berlin/Zeuthen PHE 77-2 (1977)
6. Hydra system manual, CERN Program Library (1971)
7. H. Baerwolff et al.: preprint IHEP-Berlin/Zeuthen PHE 86-04 (1986)
8. R. Gatto et al.: Phys. Lett. 170B (1986) 1
9. J. Ranft, S. Ritter: Z. Phys. C – Particles and Fields 26 (1983) 347; J. Ranft, S. Ritter: Z. Phys. C – Particles and Fields 27 (1985) 413
10. S.J. Brodsky: Proceedings of Summer Institute on Particle Physics, p. 133, Stanford, 1979
11. U. Becker et al.: Phys. Rev. Lett. 37 (1976) 1731
12. P. Bosetti et al.: Nucl. Phys. B94 (1975) 21
13. H. Dibon: Proceedings of the XVIIth Int. Smposium on Multiparticle Dynamics, p. 595, Seewinkel, 1986